

UNCLASSIFIED

Defense Technical Information Center
Compilation Part Notice

ADP014277

TITLE: Deformation-Induced Crystallization and Amorphization of Al-Based Metallic Glasses

DISTRIBUTION: Approved for public release, distribution unlimited

This paper is part of the following report:

TITLE: Materials Research Society Symposium Proceedings Volume 740
Held in Boston, Massachusetts on December 2-6, 2002. Nanomaterials for
Structural Applications

To order the complete compilation report, use: ADA417952

The component part is provided here to allow users access to individually authored sections of proceedings, annals, symposia, etc. However, the component should be considered within the context of the overall compilation report and not as a stand-alone technical report.

The following component part numbers comprise the compilation report:

ADP014237 thru ADP014305

UNCLASSIFIED

Deformation-induced crystallization and amorphization of Al-based metallic glasses

Rainer J. Hebert and John H. Perepezko

Department of Materials Science and Engineering, University of Wisconsin-Madison, Madison, WI 53706, U.S.A.

ABSTRACT

A main requirement for the application of nanostructured materials for structural applications is their thermal stability. Structural materials are often exposed to mechanically-induced stress states. Nanomaterials for structural applications should therefore retain their microstructure not only within a defined temperature range but also under applied load. Cold-rolling experiments with melt-spun $\text{Al}_{87}\text{Ni}_{10}\text{Ce}_3$ ribbons containing a dispersion of nanocrystallites in an amorphous matrix demonstrate that during the continued deformation through repeated rolling and folding crystallization as well as amorphization reactions could be induced. The results indicate that in addition to the microstructure control through annealing of precursor materials, deformation processing represents an effective approach to the synthesis of amorphous and nanophase composite materials.

INTRODUCTION

Strengthening mechanisms based on the dispersion of second-phase particles or fibers are fundamental to many structural materials. Among the latest examples for composite materials are amorphous, Al-based alloys containing nanocrystallites. The high density (approximately 10^{21} to 10^{22} m^{-3}) of primary Al-nanoparticles or quasicrystals dispersed in the amorphous matrix contributes to an exceptional specific strength. For example, a tensile strength of 1560MPa has been measured for $\text{Al}_{88}\text{Ni}_9\text{Ce}_2\text{Fe}_1$ melt-spun ribbons [1,2]. The nanocrystallites are induced through annealing of amorphous precursor materials. Of particular interest are therefore marginal glass-formers, i.e. amorphous systems that reveal a primary crystallization reaction of Al. The temperature range for primary crystallization reactions is between 170°C and 280°C for most Al-based systems. Due to the high cooling rates of 10^5 - 10^6 Ks^{-1} that are necessary to avoid growth of nuclei or nucleation reactions during the melt-spinning process [3] bulk samples can not be processed directly for the alloys used so far.

Current efforts to produce bulk amorphous Al alloys focus mainly on the compaction and extrusion of amorphous, atomized powders [4,5]. In many cases the deformation of amorphous phases was observed to yield a crystallization reaction, for example upon cold-rolling of Al-Y-Fe and Al-Sm based amorphous ribbons [6], upon bending of different Al-based amorphous ribbons [7], warm-extrusion of gas-atomized amorphous powders [4,5] if the extrusion ratio exceeds a critical value or nanoindentation of a Zr-based glass [8]. A different approach towards bulk amorphous nanocomposites is the continued rolling and folding of crystalline, elemental multilayer arrays [9,10]. After several rolling and folding cycles of Al-Sm multilayer samples, for example, a glass-transition could be detected [11]. The observation of cold-rolling induced crystallization reactions of melt-spun amorphous ribbons on one hand and the amorphization of crystalline multilayers on the other hand suggests that a cyclic crystalline-to amorphous transformation might occur during the deformation processing, similar to the cyclic

transformation behavior of ball-milled Co-Ti and Al-Zr powders [12]. In this work results of rolling experiments with partially crystalline $\text{Al}_{87}\text{Ni}_{10}\text{Ce}_3$ ribbons are highlighted. The partially crystalline structure of the $\text{Al}_{87}\text{Ni}_{10}\text{Ce}_3$ ribbons is useful in testing whether the crystalline fraction in the amorphous matrix is enhanced or dissolved with cold-rolling. The rolling of the ribbons serves therefore as a tool for a systematic investigation of changes in the microstructure and the crystallization behavior upon deformation.

EXPERIMENTAL PROCEDURE

Melt-spun ribbons with a length of about 2.5cm, each, were aligned parallel to each other as a first layer. Shorter ribbon pieces were then arranged in a second layer on top of the first layer such that the shorter ribbons in the second layer were perpendicular to the first layer and covered the ribbons of the first layer entirely. This bilayer sample was then rolled between steel sheets in a first step. This process leads to flow and compaction of the ribbons into one piece. Afterwards, the piece was rolled directly in the rolling mill at the highest deformation level (distance between the rollers set to zero). Then the piece was cut into 2 or 3 smaller pieces that were subsequently stacked on top of each other. This stacked array was then rolled again between steel sheets, and eventually without the sheets, directly in the mill. This procedure was then repeated. The strain was calculated by measuring the thickness after the stacking, before the rolling, and after the rolling. For example, when the thickness after the stacking was 3 units and after the rolling 1unit, the strain was determined as $\ln 3$.

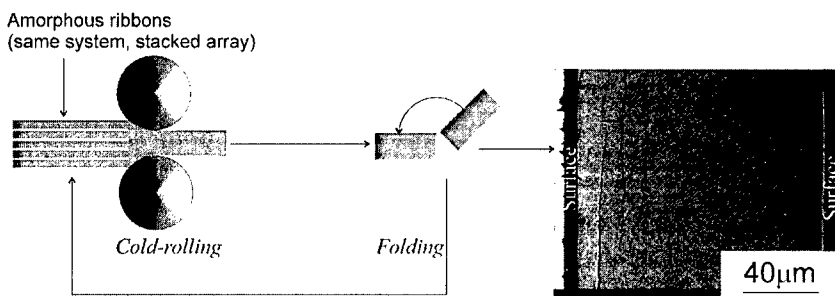


Figure 1. Schematic illustration of the folding and rolling process (left). The SEM image (right) depicts a cross-section of $\text{Al}_{85}\text{Ni}_{10}\text{Ce}_5$ ribbons that were processed according to the schematic illustration. The strain for the sample is approximately -10 .

The X-ray analysis was performed with a Cu-K α source, the DSC results were obtained in a Perkin-Elmer DSC-7 system. For the TEM analysis, samples were ion-milled at a final milling angle of 11° with a total current of approximately 2.5mA. All samples were cooled with liquid nitrogen during the TEM sample preparation. The TEM images were taken with a Philips CM-200 TEM. All ribbons were melt-spun in a single-roller melt-spinner with a copper wheel of 30cm in diameter and a wheel-speed of 55m/s. All ribbons used for the rolling experiments were examined by XRD for crystallinity prior to the rolling. For the experiments that entailed a comparison between as-spun and cold-rolled ribbons from the same system, different pieces

from the same ribbon have been used for all experiments. This ensured that the structure of the samples prior to the experiments were nearly identical.

The rolling procedure is illustrated schematically in figure 1. Added in figure 1 is a SEM cross-sectional image of an $Al_{85}Ni_{10}Ce_5$ melt-spun sample that was cold-rolled several times to a total strain of approximately -10 . The thickness of the sample in figure 1 is approximately $130\mu m$ while the initial ribbon thickness was about $30\mu m$. The SEM image shows that aside from two cracks no layer structure is visible suggesting that this method of repeated folding and rolling of ribbons is capable of providing sheet material.

RESULTS

Partially crystalline melt-spun $Al_{87}Ni_{10}Ce_3$ ribbons were selected for the current experiment (figure 2(a)). In addition to a broad amorphous peak, the Al(111) and Al(200) peaks are visible as well as additional peaks with low intensities. The X-ray patterns of the cold-rolled samples demonstrate that the crystalline fraction in the sample decreases until crystalline peaks are no longer visible at a strain of approximately -4.3 and -7.9 . In the X-ray patterns of the samples that were rolled at a strain of -4.3 and -7.9 a distinctive shoulder is observed at an angle of $45^\circ 2\theta$.

The isochronal DSC traces for the as-spun and cold-rolled samples are shown in figure 2b. The trace of the as-spun ribbon reveals a strong exothermic signal at temperatures below $110^\circ C$ followed by a primary crystallization reaction with an onset of $180^\circ C$. At $340^\circ C$ an additional exothermic reaction occurs. The analysis of the peak onset for the primary crystallization peak shows a decrease in the onset temperature from $180^\circ C$ to $175^\circ C$ at a deformation level of -4.3 . Upon further deformation the onset temperature of the primary crystallization peak shifts to approximately $150^\circ C$ while the minimum of the peak decreases only from $200^\circ C$ to $195^\circ C$, i.e. the primary crystallization peak broadens.

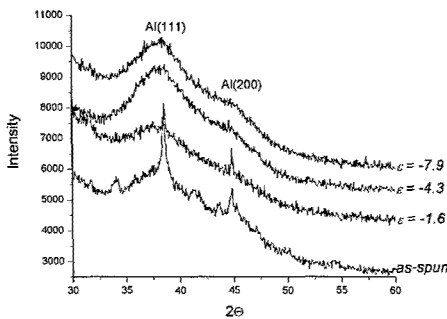


Figure 2(a): X-ray patterns of the $Al_{87}Ni_{10}Ce_3$ ribbons in the as-spun state and at different cold-rolled levels.

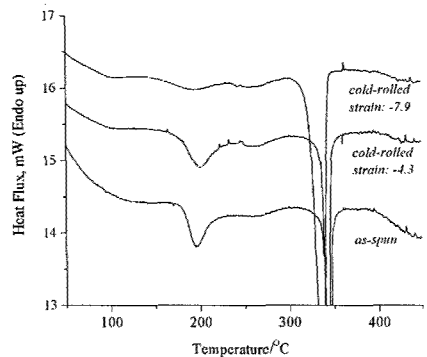


Figure 2(b): DSC traces of as-spun ribbon and after cold-rolling (heating rate $20K/min$).

From the XRD measurements it is evident that the as-spun sample contains at least two crystalline phases that gradually vitrify during the rolling process. The shift of the primary

crystallization peak in the DSC trace to lower temperatures between the sample rolled at -4.3 and -7.9 is similar to the behavior observed for the $\text{Al}_{88}\text{Y}_7\text{Fe}_5$ sample that was fully amorphous in the as-spun state but crystallized with rolling [6]. This suggests that the $\text{Al}_{87}\text{Ni}_{10}\text{Ce}_3$ sample could crystallize with further rolling once the crystalline phases have dissolved. The bright-field (BF) TEM images in figures 3-6 help to gain a better understanding of the deformation-induced structural changes in the sample. Figure 3 depicts the as-spun sample. It is apparent that crystallites exist on two different size-scales: one class with a size in the 7-15nm range, the size range of the bigger particles between 25nm and approximately 100nm (particles with a size of about 100nm were observed, but are not shown in the image). In figure 4 three different positions of the sample rolled at a strain of -1.6 are shown. Figure 4(a) is similar to the structure of the as-spun sample. Figure 4(b) shows a transition between a structure similar to the as-spun sample and a structure with very small particles (mostly $<6\text{nm}$). Moreover, the dark particles in the transition region (indicated by arrows) reveal an elongation in the same direction. A similar directionality is observed in figure 4(c). Here, the particles are not only elongated, but

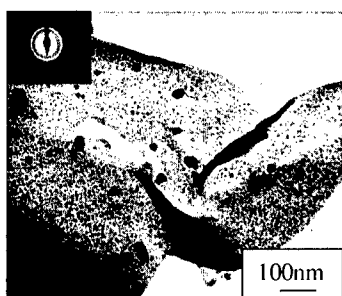


Figure 3: BF-TEM image of as-spun $\text{Al}_{87}\text{Ni}_{10}\text{Ce}_3$ ribbon. Inset shows selected area electron diffraction pattern (SAEDP).

aligned in rows. The particles in the rows break into smaller units. In between the rows, nearly particle-free regions can be observed.

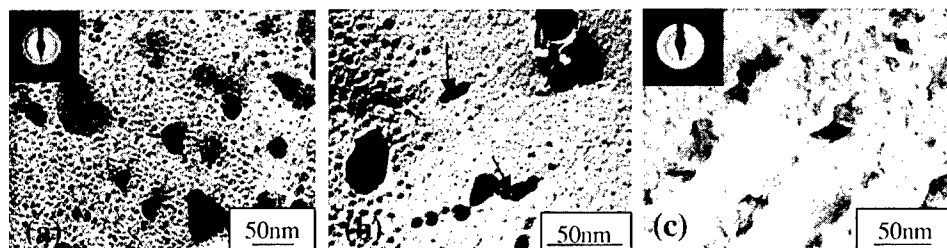


Figure 4: BF-TEM images of the rolled sample at a strain of -1.6 . Insets show SAEDP.

The electron diffraction pattern in the BF-TEM image of the sample at a strain of -4.6 (figure 5) shows that at this strain level, the sample is mostly amorphous. Although no peaks can be identified in

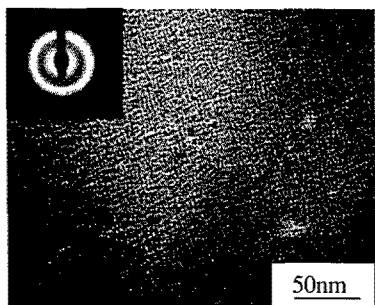


Figure 5: BF-TEM image of the sample rolled at a strain of -4.3 . Inset shows SAEDP.

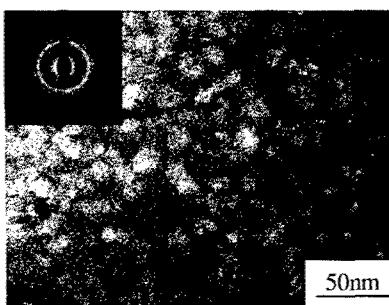


Figure 6: BF-TEM image of the sample rolled at a strain of -7.9 . Inset shows SAEDP.

the X-ray pattern, particles are observed in the TEM images, albeit at a lower density than in the as-spun state. Figure 6 demonstrates that upon continuation of the deformation to a strain of -7.9 the particle density increases again. Both, figures 4 and 5 are representative for the microstructures at the respective strain levels as the survey of several different locations in the sample during the TEM monitoring indicated.

DISCUSSION

The main shift in the onset temperature of the DSC primary crystallization peak occurs in the $\text{Al}_{87}\text{Ni}_{10}\text{Ce}_3$ sample between a strain of -4.3 and -7.9 . At a strain of -4.3 the shift in the onset of the primary crystallization temperature is only 5K towards lower temperatures, but at a strain of -7.9 the onset temperature has shifted about 20K towards lower temperatures compared with the onset temperature of the as-spun sample. The X-ray and TEM experiments suggest that the slow change in the DSC behavior between the beginning of deformation and a strain of about -4.3 could be related to the transformation of the partially crystalline structure to an amorphous state with a low particle density (figure 5). The mechanism of this transformation appears to be based on a deformation-induced elongation of the particles with subsequent rupture. This would mean that the particles that crystallized during the melt-spinning process can undergo plastic deformation. Figure 4 furthermore demonstrates that during the deformation-induced dissolution of the particles at a given strain only parts of the samples are transforming while other parts still retain their as-spun structure (figure 4, left image). This is in agreement with the idea of localized deformation of amorphous structures in shear-bands at lower temperatures [13]. However, the lateral extension of the areas revealing a band structure as displayed in figure 4, right image, is of the order of several hundred nanometers. The thickness of shear-bands in bent $\text{Al}_{90}\text{Gd}_5\text{Fe}_5$ ribbon is reported to be 10-15 nanometers [14]. The transformation does therefore not proceed in individual shear-bands.

An important finding is the observation that the dissolution of the crystalline phases with rolling is converted at higher strain levels. The selected area electron diffraction pattern (SAEDP) in figure 6 shows clearly the presence of crystalline particles while the SAEDP in figure 5 is more indicative of an amorphous phase. A cyclic crystalline-to amorphous transformation behavior was observed for ball-milled Co-Ti or Al-Zr [12] powders suggesting that upon further deformation of the ribbons the crystalline fraction might decrease again, but the strain regime beyond a strain of -8 has not yet been explored.

As an alternative to a cyclic transformation behavior the microstructure of the ribbon may evolve towards a steady-state that depends on the external forcing condition that scales with the strain-rate as well as on an average relocation distance per strain increment which is a material property [16]. For the strain-rate used in the rolling experiments the steady-state structure would be an amorphous phase containing Al nanoparticles with a size of about 5-20nm as observed for $\text{Al}_{88}\text{Y}_7\text{Fe}_5$ ribbons [6] and in this work for $\text{Al}_{87}\text{Ni}_{10}\text{Ce}_3$ partially crystalline ribbons.

SUMMARY

Cold-rolling experiments with melt-spun $\text{Al}_{87}\text{Ni}_{10}\text{Ce}_3$ ribbons containing fcc-Al nanocrystals and an additional crystalline phase dispersed in an amorphous phase resulted in an amorphization reaction followed by an increase in the crystalline fraction with continued rolling. The results show that the microstructure during the amorphization reaction is heterogeneous. While some areas reveal a banded structure with particles aligned in rows that are parallel to each other, some parts of the sample are not yet affected by the deformation. The TEM images suggest that the amorphization reaction occurred by deformation-induced fracture/rupture of the particles in the matrix. The rolling experiments with melt-spun amorphous Al-based alloys show that deformation processing offers the opportunity to control their microstructure.

ACKNOWLEDGEMENTS

The continued support and encouragement of Dr. W. Mullins, Army Research Office, for the study of the deformation-induced crystallization behavior of Al-based amorphous materials is most gratefully acknowledged (DAAD 19-01-1-0486).

REFERENCES

1. Y.H. Kim, A. Inoue, T. Masumoto, *Mat. Trans. JIM* **31**, 747 (1990).
2. Y.H. Kim, A. Inoue, T. Masumoto, *Mat. Trans. JIM* **32**, 599 (1991).
3. J.H. Perepezko, R.J. Hebert, *JOM* **54**, 34 (2002).
4. Y. Kawamura, H. Kato, A. Inoue, T. Masumoto, *Int. J. Powder Met.* **33**, 50 (1997).
5. D.J. Sordelet, E. Rozhkova, P. Huang, P.B. Wheelock, M.F. Besser, M.J. Kramer, M. Calvo-Dahlborg, U. Dahlborg, *J. Mater. Res.* **17**, 186 (2002).
6. R.J. Hebert, J.H. Perepezko, *Mater. Sci. Engr. A* (in press).
7. H. Chen, Y. He, G.J. Shiflet, S.J. Poon, *Nature* **367**, 541 (1994).
8. J.-J. Kim, Y. Choi, S. Suresh, A.S. Argon, *Science* **295**, 654 (2002).
9. M. Atzmon, J.D. Verhoeven, E.D. Gibson, W.L. Johnson, *Appl. Phys. Lett.* **45**, 1052 (1984).
10. F. Bordeaux, A.R. Yavari, P. Desré, *Mat. Sci. Engr.* **97**, 129 (1988).
11. G. Wilde, H. Sieber, J.H. Perepezko, *Scripta Mat.* **40**, 779 (1999).
12. M. Sherif El-Eskandarany, "Mechanical Alloying" (William Andrew Publishing, 2001), pp. 209-225).
13. C.A. Pampillo, *J. Mater. Sci.* **10**, 1194 (1972).
14. Y. He, G.J. Shiflet, S.J. Poon, *Acta Met. Mat.* **43**, 83 (1995).
15. M. Sherif El-Eskandarany, K. Aoki, K. Sumiyama, K. Suzuki, *Acta Mat.* **50**, 1113 (2002).
16. R.A. Enrique, P. Bellon, *Phys. Rev. Lett.* **84**, 2885 (2000).

**Modeling, Simulations,
and Interfaces**